Astronomical Objects Classification by Convolutional Neural Network Algorithms Layers

Daniel Kyselica
Faculty of Mathematics Physics and Informatics
Comenius University in Bratislava
Bratislava, Slovakia
daniel.kyselica@fmph.uniba.sk

Linda Jurkasová
Faculty of Mathematics Physics and Informatics
Comenius University in Bratislava
Bratislava, Slovakia
linda.jurkasova@fmph.uniba.sk

Roman Ďurikovič
Faculty of Mathematics Physics and Informatics
Comenius University
Bratislava, Slovakia
durikovic@fmph.uniba.sk

Jiří Šilha
Faculty of Mathematics Physics and Informatics
Comenius University in Bratislava
Bratislava, Slovakia
jiri.silha@fmph.uniba.sk

***Abstract*—Our work focuses on application of modern experimental Machine Learning (ML) algorithms toward the space objects classification. Two types of data are analyzed, frame objects present on the astronomical Flexible Image Transport System (FITS) frames and space objects' light curves, which could be considered as a footprint for given object. In our work we will present ML algorithm used for recognition of frame objects present in the FITS frames by using their specific shape. Presented algorithm is a Convolutional Neural Network (CNN) of 9 layers. The input to the network is a small 50x50 image which must contain only one object for the network to correctly classify it. This could later be used as subnet in region-based CNN after finding regions of interest in full FITS image. Additionally, we present results of applying CNN neural network based on ResNet architecture to classify light curves to categories based on their shape. For deep learning we used primarily public catalogue light curves of selected populations of upper stages e.g., Falcon 9, Atlas Centaur 5, Delta 4 which usually contain simpler features in their photometric series. The modeling software Blender was also used to generate synthetic light curves for training purposes. Algorithm can identify correctly more than 84% of tested objects. In near future we plan to extend the algorithm to identify more complex objects such as box-wing and single box-wing satellites.**

Keywords—light curves, frame objects, classification, machine learning

I. Introduction

Space debris population is constantly increasing, and its regular monitoring allows to secure safety operation in space for manned and satellites missions. The large amount of data constantly acquired for space objects allows to create sufficient number of training data sets for modern Machine Learning-based methods to help to characterize the objects according to their detected signal.

A. Space Debris Observation

Optical passive observations conducted by ground-based [1] and space-based optical sensors [2] are one of the primary sources of information concerning the space objects' dynamical (positions, orbits, rotation) and surface properties. Raw output products of such observations are frames in format of Flexible Image Transport System (FITS) [3] which are acquired with Charge Coupled Device (CCD) or Complementary Metal Oxide Semiconductor (CMOS) detectors. FITS frames contain different sources of signal including the signal from the object of interest (space debris, satellite, minor planet, etc.), which is then further processed. Applied processing methods to FITS frames depend on the overall objective. The astrometry is procedure when the object's relative position on the sky is extracted. These positions are then used for orbit determination or improvement [4]. The photometry focuses on acquisition of object's brightness and its change over time, referred to also as light curves. These data are used to characterize the space objects [5] and to determine their attitude states [6].

Some features present on the FITS frames could be used to calibrate the information about the object of interest. The reference stars are used to determine the object's astrometric position and/or standard brightness. The background noise is measured to estimate the measurement error. However, features like "cosmics", a group of bright pixels created from interaction between highly energetic particles with the detector's chip, or features like galaxies, which are diffuse sources, could be considered in the view of space debris observations as unwanted signal. Usually, the analytical segmentation algorithms are responsible to distinguish those features in FITS frames [7].

One type of data obtained from optical observations are light curves. They contain information about the object's shape, size, surface reflectance properties, and object's own rotation/tumbling [5]. Such a footprint can be unique for different types of populations, e.g., upper stages, satellite build, debris fragments. Therefore, they can be used for object classification and characterization if they processed properly.

B. Machine Learning and Convolutional Neural Networks

Machine learning (ML) field focuses on creating system capable of adapting automatically through experience according to [8]. Machine learning can learn patterns hidden inside this data and help us to use it as a powerful tool. Neural networks are part of this field. Neural network propagates input through layers of perceptrons (individual units) that use nonlinear activation function between layers.

Convolutional neural networks (CNNs) are special kind of neural networks [9] for processing data with grid-like topology. For example, images can be perceived as 2D grid of pixels and time series as 1D grid of individual measurements in time. CNN uses convolution instead of matrix

ESA Contract No. 4000136672/21/NL/SC "Validation of re-entry models by using real optical measurements obtained by AMOS global network (Amos-Reentry)". Additional funding by Comenius University, UK/279/2022.

multiplication with at least one of its layers. Convolutional layers are able to learn features presented in training data and the convolutional process is shown in the Fig. 1. Kernel of chosen size is applied to an image repetitively with chosen stride. Output is an image with size depending on stride and kernel size.

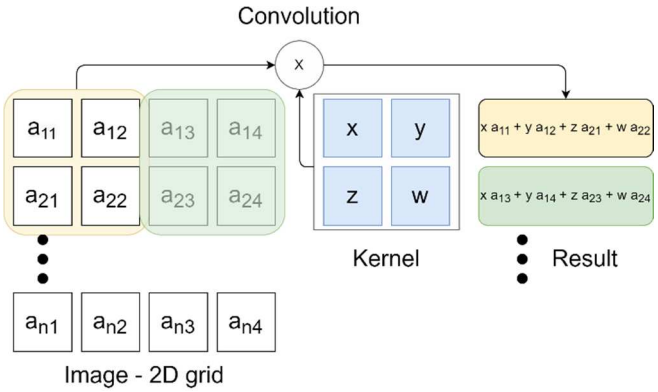

Fig. 1. Process of convolution. Kernel is applied to parts of an image.

CNNs became the best solution for image classification in 2012 when AlexNet [10] won the ImageNet Large Scale Visual Recognition Challenge (ILSVRC). ILSVRC [11] contains 14 million labeled training images with over 20,000 categories. Unfortunately, there are no image space images in the dataset to be used in training, therefore the straightforward application of ML approaches may not be possible. Competitors must classify at least millions of testing examples to corresponding classes. 2012 winner Alexnet finished with 15.3% top-5 with error 10% less than other systems.

Large CNN models are computationally very expensive. AlexNet authors [10] have introduced revolutionary solution to train these kind of networks using (Graphical Processing Units) GPUs which made training of large models feasible. Since then CNNs are used for various computer vision tasks.

C. *Machine Learning Application on Light Curves*

Acquiring information about objects' properties such as their movement, rotation and material is helpful for their classification and potential removal. Light curve, an object's footprint, consists of object's flux observations in time and carries information about its properties. By analytical methods used in astronomy, it is possible to methodically obtain limited information from light curves. However, there are parameters which are being neglected and can be key to more detailed classification or description of the object.

In recent studies CNNs are used to solve the problem mentioned in the article [12]. The neural network takes light curve as input to be classified based on the object's shape. For properly trained neural network fair amount of good quality data is required. One of the options is to synthetically generated data. In the article [13] Cook-Torrance Bidirectional Reflectance Distribution Function (BRDF) was used in photometric models of space debris. The model needs the reflectance parameters to be specified, that is of course possible but with precise measurement on ground.

The authors in [12] chose different approach. Synthetic light curves are generated using modeling software Blender. Main advantage of this approach is control over all of the properties of a simulated object. 3D models of real objects are freely available on NASA's website [14]. Additionally, 3D models of satellites with yet nonexistent shapes can be constructed which would enable CNN to identify satellites deployed in the future.

Another proposed type of neural network is Recurrent Neural Network (RNN) in [15]. RNNs can process sequences of inputs and learn dependencies between inputs in time. Due to this fact they are commonly used for problems in natural language processing domain. On the contrary, their accuracy of light curves classification was far below CNN's.

D. *Machine Learning Application for Space Object Recognition*

FITS frames acquired during astronomical observations contains different types of frames objects and must be processed in multiple steps: object detection, feature extraction, and finally classification. For many years, traditional methods were used for this task. However, with the huge increase in the amount of data, there is a need for fast, robust, and automatic tools to perform some of the data processing. As the popularity of ML models has spread widely across many fields of study, the astronomical field has adapted some of the technologies as well.

One of the most common tasks, when it comes to object recognition is star/galaxy classification. This area has been researched very thoroughly by many professionals. In [16], the authors used three different Neural Networks (NNs) for each specific task. First, the non-linear Principal Component Analysis Neural Networks (PCA NN) was applied to the image, which reduced the redundant information in nearby pixels. Transformed values of the pixels were then fed to unsupervised NN, which performed image segmentation. Afterward, the best-performing features were selected using a sequential backward elimination strategy. These were then used to train Multi-Layer Perceptron (MLP) for the final task of star/galaxy classification.

A different approach to star/galaxy classification was presented in [17]. Instead of three separate NNs, the authors used the Mask Region-Based Convolutional Neural Networks (RCNN) framework (with ResNet-101 as a backbone) to perform all tasks. Transfer learning was used to improve the training process, with weights trained on the Microsoft COCO dataset.

Another task prevalent in the astronomical field is the classification of various types of galaxies. In [18] five different ML methods were chosen to test the best performing strategy: Decision trees, K-nearest neighbors, Random Forest, ExtraTrees, and Artificial Neural Network (ANN). In contrast to the previously mentioned articles, features weren't extracted from the image by the authors but instead retrieved from the Sloan Digital Sky Survey database. Evaluating the models on the testing set and comparing the accuracy showed that ANN had the best results when the dataset is balanced.

II. Training, Validation and Test Data

A. *Light Curves - Real Data*

Primary source of training data for our work are publicly available light curves from Mini Mega Tortora (MMT) which is wide-field monitoring system with nine channels for optical observations of the sky, mounted in pairs on five stands and is operated by Special Astrophysical Observatory of Russian Academy of Sciences, Russia [19]. Every track in the catalogue contains: light curves in standard and apparent

magnitudes, distance, phase angle over time, light curve period, whether the object was in penumbra, etc. The MMT database contains 3662 objects, from which 1388 (37.9%) are stable (observed no apparent rotation), 1366 (37.3%) are slow rotators (rotation observed but no apparent rotation period could be extracted) and 908 (24.8%) are rotators (apparent rotation period could be extracted) (to April 2020).

In Fig. 2 top shows the light curve for US upper stage Falcon 9 R/B with international ID 15023D (Norad ID 40618) published by MMT. Apparent rotation period has been extracted from the light curve and used to constructed folded light curves, so-called phase diagram plotted in Fig. 2 bottom.

As a complementary to MMT catalogue we can use the Space Debris Light Curve Database (SDLCD) catalogue of the Faculty of Mathematics, Physics and Informatics, Comenius University in Bratislava (FMPI) which contains processed data observed on Astronomical and geophysical observatory in Modra [1]. The main catalogued objects are on geosynchronous and eccentric orbits with planned extension to Low-Earth Orbits (LEO) [5]. SDLCD contains (to date April 2020) in total 543 tracks (light curves) for 356 individual objects. All tracks are in arbitrary instrumental magnitude system and are not reduces to standard system. From 543 tracks, 512 showed periodic signal and the apparent rotation period could be extracted and the rotation phase could be constructed for them.

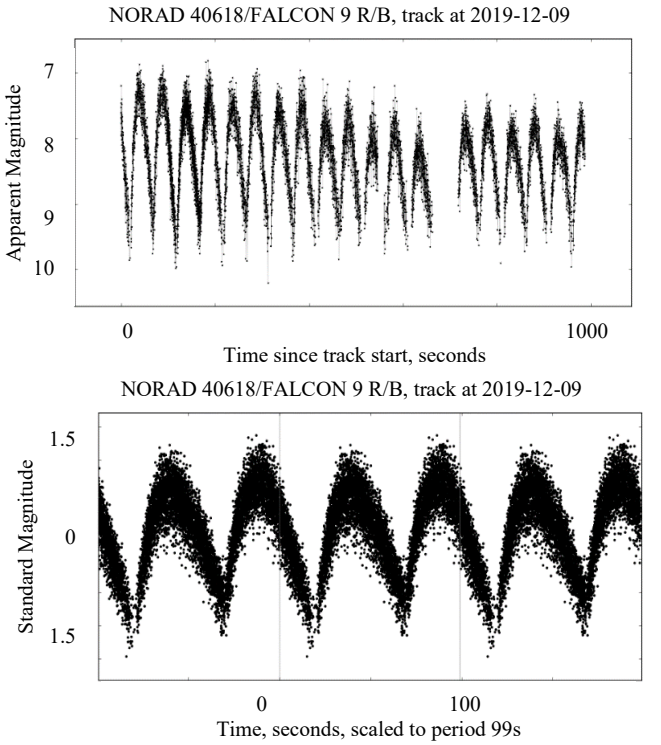

Fig. 2. The light curves. Top: Example of light curve for Falcon 9 R/B (15023D, 40618) published in MMT [19]. Bottom: Folded phase diagram for Falcon 9 R/B assuming apparent rotation period = 132.8 s.

B. *Light Curves – Synthetic Data*

For purposes of training neural network fair amount of training data is needed. Unfortunately, public catalogues seem to have not yet sufficient amount of real light curves for larger number of populations. To tackle this issue we are presenting system capable of generating synthetic light curve with use of open source modeling and rendering software Blender [20]. The python script API for Blender was used to create modeling movement of Sun, observer, and moving object. Sun and observer realistic movements include Earth's rotation around its axis and Sun. Movement of orbiting object around Earth is described by Keplerian elements. Another parameters are axis of object rotation and its period. Frame is rendered using camera view for every time step as in Fig. 3. Frames like these are saved for further processing.

To create light curve, total intensity is computed for each rendered frame representing flux measurement in time. Generated light curves follow patterns similar to real light curves, without presence of a noise. Fig. 4 shows how similar real and synthetic light curves of box-wing satellites with two solar panels are. Two main sharp spikes are visible in both light curve, for the real one plotted in Fig. 4 left and the synthetic one plotted in Fig. 4 right.

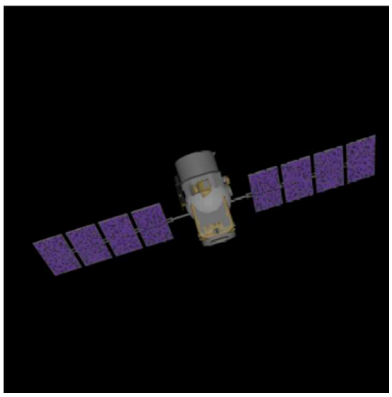

Fig. 3. Calipso satellite in modeling software Blender. Model obtained from [14].

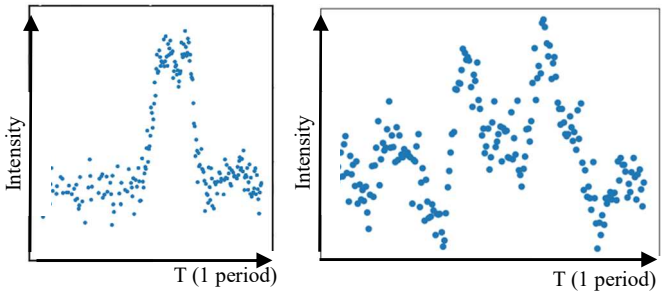

Fig. 4. Comparison of real and synthetic light curve. Pictures show one rotation period of satellites. Left: Real light curve of Navstar (GPS) satellite from MMT database. Right: Synthetic light curve of Calipso satellite created by our system.

C. *FITS Frame – Real Data*

Most of the real images used in this work are acquired from the Astronomical and Geophysical observatory in Modra. As these are ground-based observations focused on tracking space debris, the most prevalent features present on the images are Resident Space Objects (RSOs) like satellites, space debris. Other often present objects are stars and occasionally galaxies and comets. Depending on the relative position and dynamics between the observer and the object of interest, signals from RSOs can either appear as a point or a streak. An example of the two full-frame images can be seen in the Fig. 5.

The shape of the point source is defined by the point spread function also called PSF. The function is usually circularly symmetric and can be approximated using a central Gaussian

core. To express the size of the PSF, Full Width at Half Maximum (FWHM) is used, which measures the diameter of the Gaussian core in half of its maximum amplitude [21].

RSO can also appear as a streak, which resembles a line. Streak is approximated using multiple point-spread functions moving at a constant rate in one direction and forming a line. This function is referred to as PSF-Convolution Trail Function. A streak-like feature can be described by its length, orientation, and width [21].

Another prominent feature present in the images is a galaxy. Based on their visual appearance galaxies can be classified into 4 categories: elliptical, spiral, lenticular, and irregular. In this work, our focus is on elliptical galaxies. One of the main characteristics of elliptical galaxies is that they are highly concentrated and the light going from the center fades smoothly and rapidly away, which creates a smooth diffuse profile. We can measure their degree of ellipticity, which is defined by the ratio of minor to major diameter [23].

Apart from RSOs and other stellar bodies, the images also contain many various defects and noises. By their nature, they can be distinguished into 2 categories: internal and external. Internal are caused by issues within the CCD chip. This includes noises like bias, readout noise, dark current, and some defects such as hot and dead pixels, dead columns, traps, etc. On the other hand, external noises are caused by external forces such as moonlight, sunlight, atmosphere. This includes one of the most dominant sources of noise – sky background noise and others like stray light or cosmic rays.

The input to our trained CNN is an image of size 50x50 pixels. For this reason, real full-frame image is cut to size of 50x50 pixels, where a single object is present, see Fig. 6.

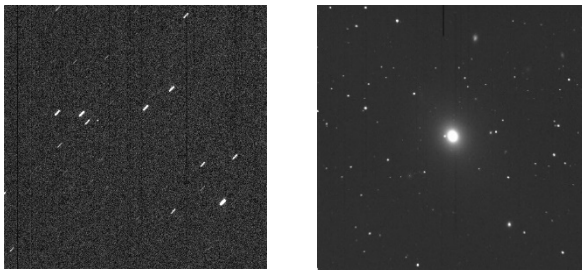

Fig. 5. An example of images acquired in AGO. On the left image, stars appear as streaks and the object of interest has a point-like shape. The right image shows an elliptical galaxy and point-like stars.

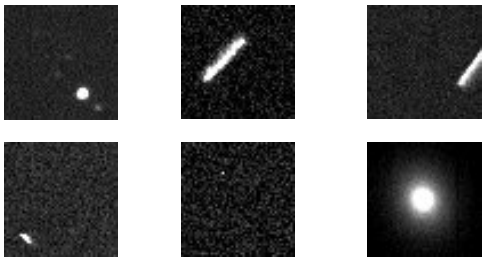

Fig. 6. Examples of 50x50 pixel cutouts from real images. Top row from left: a point, a streak, a cut streak. Bottom row from left: a cosmic ray, a hot pixel, a galaxy.

D. FITS Frame – Synthetic Data

The neural network training requires a fair amount of data, which is not available. However, this issue can be easily solved with a generator of synthetic images. The department of Astronomy and Astrophysics, FMPI has its generator - starGen, which was improved and extended for this work. StarGen allows us to generate a series of multiple FITS images of various sizes. The script is also producing TSV files containing positions of objects on each image. The script can generate stars and multiple RSOs, which can either appear as streaks or points. It also supports the generation of elliptical galaxies.

As mentioned in the previous section point is approximated with point-spread function. In our case, we used the symmetrical Gauss function. In the configuration file, the user can define the FWMH of the PSF and the peak brightness of the object. As for the streak, the same PSF is used, which is moved in one direction to create a streak-like shape. Apart from FWHM and brightness, other parameters such as the half-length and orientation of the streak are defined in the configuration file.

To simulate elliptical galaxies, we decided to use a linear combination of two bivariate Gaussians. The first Gaussian is used to simulate the highly concentrated center of the galaxy. It has a significant peak and has a small FWHM, which makes the base very narrow. The second Gaussian simulates the outer diffuse part, with a much bigger FWHM but no obvious peak. Using bivariate Gaussian allows us to make the elliptical shape of galaxies. All the parameters like FWHM on the x and y-axis, peak brightness, and orientation can be defined for both Gaussians in the configuration file.

To make synthetic images look realistic, noises and defects needed to be added as well. Sky background noise is simulated using a normal distribution with adjustable mean value and standard deviation. To imitate the statistical probability of photons falling onto a CCD chip, Poisson noise is applied to all features. The script also supports noises such as bias, dark current, readout by uploading real BIAS, DARK and FLAT FIELD frames, which are then applied to the image. Furthermore, we also added simulation of cosmic rays. These are generated using an iterative stochastic method of assigning intensity values to specific pixels. Based on [24] we distinguish 3 types of cosmic rays: spots, tracks, and worms.

An example of a generated image using the starGen script can be seen in Fig. 7. However, for purposes of this work, only 50x50 cutouts with single object are required. Examples of some cutouts are shown in Fig. 8.

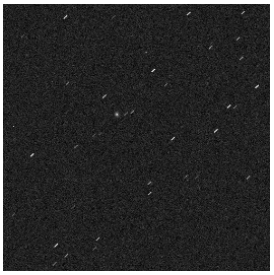

Fig. 7. Synthetic image generated with a script.

III. Object Characterization throught Light Curves

In this section we present a system for object characterization through light curve classification. Convolutional neural network can be trained to distinguish between different classes of objects and provide information about their shape.

A. *Proposed CNN Architecture*

Architecture based on ResNet [25] was used. Proposed network contains single residual block as in the Fig. 9. Therefore, it can be described as shallow residual network. Training and validation demonstrate that proposed architecture can solve assigned problem.

1D array representing one rotation period of an object in light curve is passed to CNN as input. The output of the network consists of input probabilities belonging to corresponding class C_i.

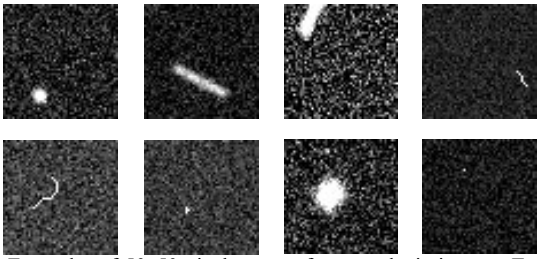

Fig. 8. Examples of 50x50 pixel cutouts from synthetic images. Top row from left: a point, a streak, a cut streak, a cosmic ray i.e. track. Bottom row from left: a cosmic ray i.e. worm, a hot pixel i.e. spot, a galaxy, a hot pixel.

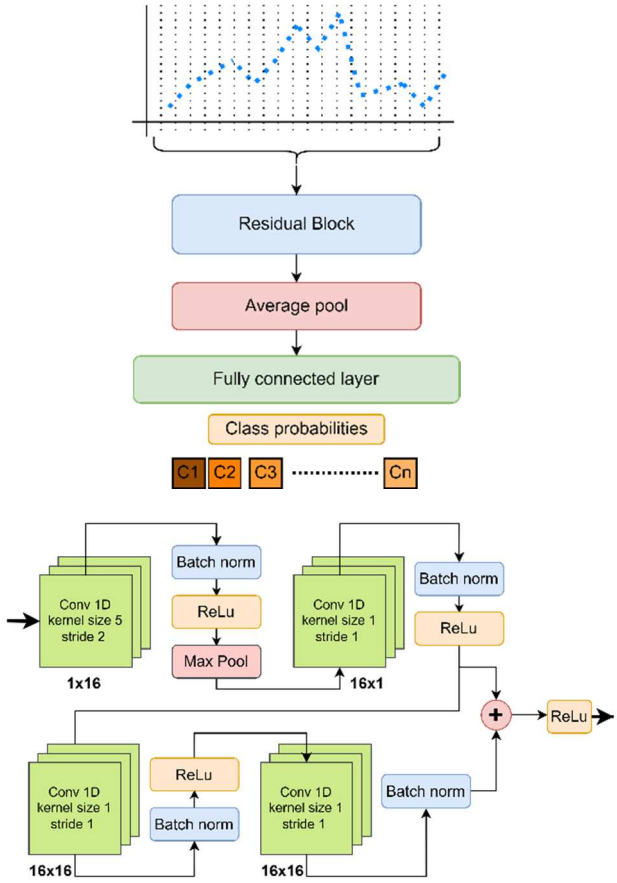

Fig. 9. Proposed architecture of convolutional neural network. Top: High level view of architecture. Bottom: Composition of residual block. Plus sign stands for element-wise addition.

B. *CNN Training*

For training purposes real light curves from MMT database (section II.A) were used. They are of different lengths and capture multiple object rotation periods. Therefore, they are transformed to data suitable for neural network. A light curve is cut to individual rotation periods and reshaped to uniform size using smoothing operations. However, in most cases light curves did not contain measurement for entire rotation periods. In many cases only 10% of them were covered. Hence, only small portion of retrieved data were suitable for training.

CNN was trained to classify light curves with high quality. Three types of objects were chosen: Falcon 9 (2000+ light curves), Atlas 5 (8000+ light curves), Delta 4 (500+ light curves). Specification of the training set demonstrates its unbalanced character. All mentioned objects are rocket bodies with similar light curve pattern which makes classification task even more difficult.

Neural network was trained for 150 epochs. Fig. 10 top shows declining trend in loss value and Fig. 10 bottom shows increased accuracy up to 88% during training.

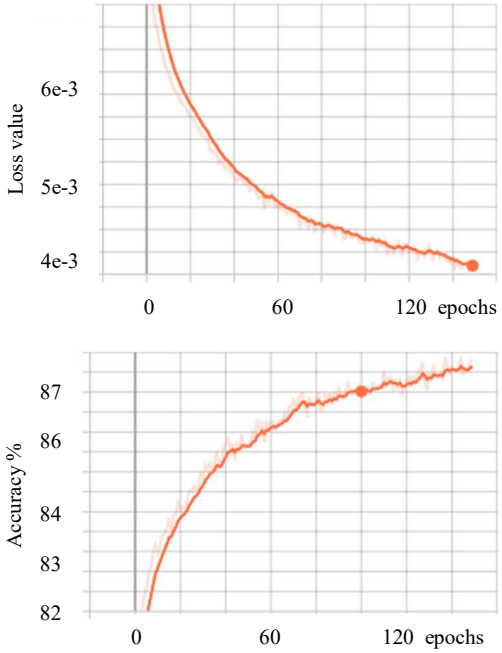

Fig. 10. Output behaviour of training accuracy and loss over 150 training epochs. Top: Training loss. Bottom: Training accuracy.

C. *CNN Testing*

To test the network performance, 10% of data was put aside as validation set before training. During training the network accuracy on validation set was monitored, see Fig. 11. Training was stopped at the first sign of overfitting indicated by decreasing validation accuracy and increased training accuracy in Fig. 11 and Fig. 10 bottom, respectively.

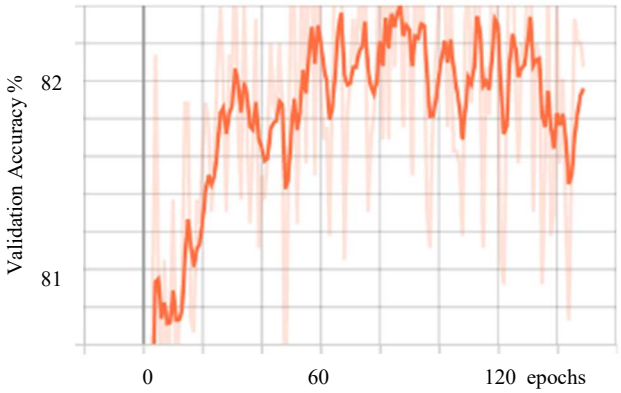

Fig. 11. Validation accuracy during training over 150 training epochs.

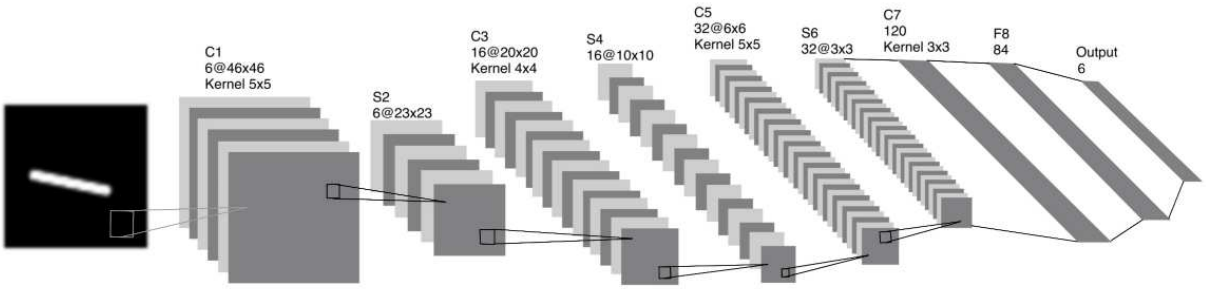

Fig. 12. The architecture of the proposed CNN. For each convolutional layer (C) the information about the kernel and size of output feature map is defined (N@MxM, where N is a number of filters used and MxM is the spatial size of the feature maps). Pooling/Subsampling layers (S) always operate with a 2x2 kernel and reduce only the spatial size of the feature maps. The last two layers of CNN are fully connected (F) and the output layer contains 6 neurons.

To test the network the data nod seen during training process by the network were used. Testing accuracy on the validation data set was above 84%.

Imbalanced number of examples in classes is huge problem with real data. Table I shows that network have great precision for Atlas 5 which is the class with highest population. On the other hand, Delta 4 was often miss-classified because the CNN was not able to learn its characteristics.

Component heads identify the different components of your paper to the style provided by the drop down menu to differentiate the head from the text. This problem can be solved using synthetic data mentioned in the Section II.B as training data. This way same number of training examples for each class can be secured. Real examples can be used afterwards to fine-tune the network.

TABLE I. CONFUSION MATRIX

True Labels	**Predicted Labels**		
	Falcom 9	***Atlas 5***	***Delta 4***
Falcom 9	147	41	6
Atlas 5	95	807	7
Delta 4	13	18	11

IV. OBJECT CHARACTERIZATION THROUGHT FRAME OBJECTS

In our work, we are focusing on object classification through FITS frames. For this purpose, we developed a convolutional neural network to extract features from the images and classify objects into correct classes. The input to our network is 50x50 pixels FITS image, where only one object is present. The outputs of the network are probability values that represent the correspondence of given input into a specific class. The network supports classification into 6 classes: point, streak, galaxy, hot pixel, cosmic ray, and cut streak.

A. Proposed CNN Architecture

For this work, we chose the traditional CNN architecture of 9 layers, which is demonstrated in Fig. 12. Convolutional layers alternate with the pooling layers and at the end of the network, there are 2 fully connected layers. The output layer of the network consists of 6 neurons, where each neuron represents a specific class.

B. CNN Training

To train the CNN, synthetic images were generated using starGen, Section II.D. The dataset was generated to be robust and cover every possible scenario. For objects, this included various brightness levels, lengths (of streaks), orientations (of galaxies and streaks), ellipticity degrees (of galaxies), or FWHM values. The training set contains 28 800 samples for each class, which gives more than 172 000 samples in total. Using generated images gives us the advantage to have control over the dataset parameters. This way we can keep the dataset balanced and robust even in the future in case our network requirements change.

The CNN was trained on 100 epochs with an early stopping algorithm deployed to prevent the network from overfitting. To find the model with the best performing parameters, the network was trained multiple times with various settings.

Fig. 13 top shows the rapid decline of both training and validation loss on the best-performing model. While Fig. 13 bottom shows the gradual increase in training and validation accuracy almost nearing 100%.

The network was trained using multiple hyperparameters. This included various activation functions, optimizers with their hyperparameters, learning rates, batch sizes, regularizations, etc. To determine the best performing settings, the validation set was used, which was evaluated after each epoch during training.

The validation dataset consists of 16 000 images for each class. The progress of validation loss and accuracy during training are shown in the Fig. 13.

C. CNN Testing

To test the performance of the network testing dataset was used. The size of the dataset is the same as the validation dataset, which gives us a total of 96 000 images. Classification accuracy on the test dataset is more than 99%. Table II shows the confusion matrix for this dataset. Based on this we can see that the network has a slight problem with distinguishing the galaxy from points or cosmic rays from hot pixels. Apart from that, the performance is impressive.

However, this dataset contains only synthetic images, and the results can be affected by this fact. Therefore, we decided to test the accuracy using cutouts from real images mentioned in Section II.C. For each class, we have collected 75 images, which gave us a dataset of 450 images. The achieved accuracy of this dataset was around 45%. However, we believe that this performance can be significantly improved using real data in the training process to fine-tune the network.

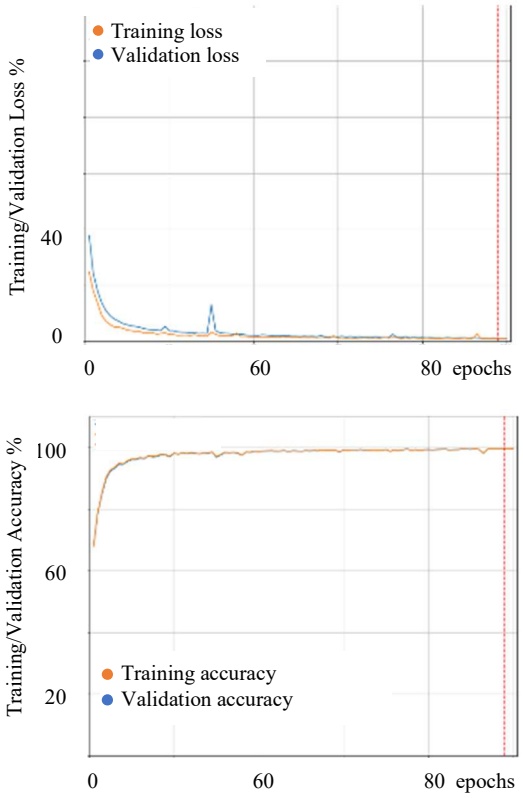

Fig. 13. Progress of training/validation loss and accuracy during training over 120 epochs. Top: Training/validation loss. Bottom: Training/validation accuracy.

TABLE II. CONFUSION MATRIX 96 000 IMAGES.

True Labels	Predicted Labels					
	Streak	***Point***	***Cut Streak***	***Hot Pixel***	***Cosmic Ray***	***Galaxy***
Streak	15883	34	14	0	0	69
Point	2	15949	4	12	4	29
Cut Streak	5	3	15928	57	7	0
Hot Pixel	0	0	4	15993	3	0
Cosmic Ray	0	0	9	82	15909	0
Galaxy	51	352	8	2	0	15587

V. CONCLUSION

In our we presented application of convolutional neural networks on astronomical data often acquired in space debris domain, light curves, and FITS frames. We implemented CNNs, the state of the art for processing images and time series, for two classification tasks.

First, we demonstrated that CNN can classify light curves based on object's shape. The network was trained using real life light curves of three rocket body groups. If big similarity of classified objects is taken in count, achieved accuracy above 84% is good starting point.

Next, we showed second use case of CNN for object characterization through frame object. For this purpose, we trained second network using synthetic images created by our generator. Network performance on synthetic data is nearly perfect, yet we were able to correctly classify about 43% of real frame objects.

To increase classification accuracy of our network we proposed new training approach. Synthetic data will be used as for training for both networks, which will ensure sufficiently large and balanced dataset. Moreover, real data will be used to fine-tune the network. We believe these approach could bring us better results in the future.

REFERENCES

[1] J. Šilha, S. Krajčovič, M. Zigo, J. Tóth, D. Žilková, P. Zigo, L. Kornoš, J. Šimon, T. Schildknecht, E. Cordelli, A. Vananti, H. K. Mann, A. Rachman, C. Paccolat, and T. Flohrer, "Space debris observations with the Slovak AGO70 telescope: Astrometry and light curves," Advances in Space Research, vol. 65, no. 8, 2020, pp. 2018–2035.

[2] V. Abbasi, S. Thorsteinson, D. Balam, J. Rowe, D. Laurin, R. L. Scott, and M. Doyon, "BVRI The neossat experience: 5 years in the life of canada's space 365 surveillance," Proceedings of ESA NEO and Debris Detection Conference, Exploiting Synergies, ESA/ESOC, Darmstadt, Germany, pp. 22 – 24, January 2019.

[3] T. F. S. Office, "Nasa flexible image transport system," [Online], May 2022. Available: https://fits.gsfc.nasa.gov/

[4] I. Molotov, V. Agapov, V. Titenko, Z. Khutorovsky, Y. Burtsev, I. Guseva, V. Rumyantsev, M. Ibrahimov, G. Kornienko, A. Erofeeva, V. Biryukov, V. Vlasjuk, R. Kiladze, R. Zalles, P. Sukhov, R. Inasaridze, G. Abdullaeva, V. Rychalsky, V. Kouprianov, O. Rusakov, E. Litvinenko, and E. Filippov, "International scientific optical network for space debris research," Advances in Space Research, vol. 41, no. 7, 2008, pp. 1022–1028.

[5] J. Šilha, M. Zigo, T. Hrobar, and P. Jevcak, "Light curves application to space debris characterization and classification," Proceedings of 8th European Conference on Space Debris, ESA/ESOC, Darmstadt, Germany, 2021, pp. 1–8.

[6] F. Santoni, E. Cordelli, and F. Piergentili, "Determination of disposedupper-stage attitude motion by ground-based optical observations," Journal of Spacecraft and Rockets, vol. 50, no. 3, 2013, pp. 701–708.

[7] V. Kouprianov, "Distinguishing features of CCD astrometry of faint GEO objects," Advances in Space Research, vol. 41, no. 7, 2008, pp. 1029–1038.

[8] M. I. Jordan and T. M. Mitchell, "Machine learning: Trends, perspectives, and prospects," Science, vol. 349, no. 6245, 2015, pp. 255–260.

[9] I. Goodfellow, Y. Bengio, and A. Courville, "Deep Learning," MIT Press, 2016.

[10] A. Krizhevsky, I. Sutskever, and G. E. Hinton, "Imagenet classification with deep convolutional neural networks," Advances in neural information processing systems, vol. 25, 2012.

[11] O. Russakovsky, J. Deng, H. Su, J. Krause, S. Satheesh, S. Ma, Z. Huang, A. Karpathy, A. Khosla, M. Bernstein, et al., "Imagenet large scale visual recognition challenge," International journal of computer vision, vol. 115, no. 3, 2015, pp. 211–252.

[12] J. Allworth, L. Windrim, J. Bennett, and M. Bryson, "A transfer learning approach to space debris classification using observational light curve data," Acta Astronautica, vol. 181, 2021, pp. 301–315.

[13] L. Yao and Z. Chang-yin, "The basic shape classification of space debris with light curves," Chinese Astronomy and Astrophysics, vol. 45, no. 2, 2021, pp. 190–208.

[14] NASA, "3d models," [Online], May 2022. Available: https://nasa3d.arc.nasa.gov/models

[15] E. Kerr, G. Falco, N. Maric, D. Petit, P. Talon, E. Petersen, C. Dorn, S. Eves, N. S´anchez-Ortiz, R. D. Gonzalez, et al., "Light curves for geo object characterisation," 8th European Conference on Space Debris, 2021, pp. 9–20.

[16] S. Andreon, G. Gargiulo, G. Longo, R. Tagliaferri, and N. Capuano, "Wide field imaging — I. Applications of neural networks to object

detection and star/galaxy classification," Monthly Notices of the Royal Astronomical Society, vol. 319, no. 3, 2000, pp. 700–716.

[17] C. J. Burke, P. D. Aleo, Y.-C. Chen, X. Liu, J. R. Peterson, G. H. Sembroski, and J. Y.-Y. Lin, "Deblending and classifying astronomical sources with mask r-cnn deep learning," Monthly Notices of the Royal Astronomical Society, vol. 490, no. 3, 2019, pp. 3952– 3965.

[18] M. Reza, "Galaxy morphology classification using automated machine learning," Astronomy and Computing, vol. 37, 2021, pp. 100492.

[19] S. Karpov, E. Katkova, G. Beskin, A. Biryukov, S. Bondar, E. Davydov, E. Ivanov, A. Perkov, and V. Sasyuk, "Massive photometry of low-altitude artificial satellites on mini-mega-tortora, IV Workshop on Robotic Autonomous Observatories (Eds. Mar´ıa Dolores Caballero-Garc´ıa, Shasi B. Pandey, David Hiriart Alberto J. Castro-Tirado)," Revista Mexicana de Astronomia y Astrofisica (Serie de Conferencias), vol. 348, 2016, pp. 112–113.

[20] B. O. Community, "Blender - a 3D modelling and rendering package," Blender Foundation, Stichting Blender Foundation, Amsterdam, 2018.

[21] W. Romanishin, "An introduction to astronomical photometry using ccds," Createspace Independent Pub, 2014.

[22] P. Vereš, R. Jedicke, L. Denneau, R. Wainscoat, M. J. Holman, and H.-W. Lin, "Improved asteroid astrometry and photometry with trail fitting," Publications of the Astronomical Society of the Pacific, vol. 124, no. 921, 2012, pp. 1197– 1207.

[23] E. Hubble, "The Realm of the Nebulae," The Silliman Memorial Lectures Series, Yale University Press, 1982.

[24] D. Groom, "Cosmic Rays and Other Nonsense in Astronomical CCD Images," Amico, P., Beletic, J.W., Beletic, J.E. (eds) Scientific Detectors for Astronomy. Astrophysics and Space Science Library, vol. 300, Springer, Dordrecht, 2004.

[25] K. He, X. Zhang, S. Ren, and J. Sun, "Identity mappings in deep residual networks," European conference on computer vision, Springer, 2016, pp. 630–645.